INFECTION AND IMMUNITY, May 2011, p. 1915–1926 Vol. 79, No. 5
0019-9567/11/$12.00 doi:10.1128/IAI.01270-10

Effect of Cytokine Interplay on Macrophage Polarization during Chronic Pulmonary Infection with *Cryptococcus neoformans*▽

Shikha Arora,[1,2,3] Michal A. Olszewski,[1,2,4]* Tiffany M. Tsang,[1,3] Roderick A. McDonald,[1] Galen B. Toews,[1,4] and Gary B. Huffnagle[1,2,3]

Division of Pulmonary and Critical Care Medicine, Department of Internal Medicine,[1] Graduate Program in Immunology,[2] and Department of Microbiology and Immunology,[3] University of Michigan Medical School, Ann Arbor, Michigan 48109-0642, and VA Ann Arbor Health System, Ann Arbor, Michigan 48105[4]

Received 1 December 2010/Returned for modification 28 December 2010/Accepted 18 February 2011

The immune response to *Cryptococcus neoformans* following pulmonary infection of C57BL/6 wild-type (WT) mice results in the development of persistent infection with characteristics of allergic bronchopulmonary mycosis (ABPM). To further clarify the role of Th1/Th2 polarizing cytokines in this model, we performed kinetic analysis of cytokine responses and compared cytokine profiles, pathologies, and macrophage (Mac) polarization status in *C. neoformans*-infected WT, interleukin-4-deficient (IL-4$^{-/-}$), and gamma interferon-deficient (IFN-γ$^{-/-}$) C57BL/6 mice. Results show that cytokine expression in the infected WT mice is not permanently Th2 biased but changes dynamically over time. Using multiple Mac activation markers, we further demonstrate that IL-4 and IFN-γ regulate the polarization state of Macs in this model. A higher IL-4/IFN-γ ratio leads to the development of alternatively activated Macs (aaMacs), whereas a higher IFN-γ/IL-4 ratio leads to the generation of classically activated Macs (caMacs). WT mice that coexpress IL-4 and IFN-γ during fungal infection concurrently display both types of Mac polarization markers. Concurrent stimulation of Macs with IFN-γ and IL-4 results in an upregulation of both sets of markers within the same cells, i.e., formation of an intermediate aaMac/caMac phenotype. These cells express both inducible nitric oxide synthase (important for clearance) and arginase (associated with chronic/progressive infection). Together, our data demonstrate that the interplay between Th1 and Th2 cytokines supports chronic infection, chronic inflammation, and the development of ABPM pathology in *C. neoformans*-infected lungs. This cytokine interplay modulates Mac differentiation, including generation of an intermediate caMac/aaMac phenotype, which in turn may support chronic "steady-state" fungal infection and the resultant ABPM pathology.

Chronic infection with *Cryptococcus neoformans* 24067 in C57BL/6 wild-type (WT) mice is an established model of allergic bronchopulmonary mycosis (ABPM) that is ideal to study mechanisms underlying immune deviation implicated in the pathogenesis of chronic fungal infections in the lungs (2, 6, 7, 18). This model can also be used to evaluate mechanisms that may counterbalance pathological processes and improve fungal clearance and to test their potential for the development of new therapeutic strategies for allergic pulmonary diseases (9, 18, 28).

The immune response in *C. neoformans*-infected C57BL/6 WT mice is predominantly Th2 biased, and this Th2 bias is thought to be responsible for the development of ABPM pathology (6, 18, 20, 28). Interestingly, the immune response to *C. neoformans* in this model is also accompanied by Th1 elements, and gamma interferon (IFN-γ) deletion results in a more severe pulmonary infection accompanied by augmented allergic responses (2). This phenotype is also associated with development of alternatively activated macrophages (aaMac) in *C. neoformans*-infected lungs (2, 6, 18), suggesting that cytokine interplay affects the process of activation of macrophages (Mac) in this model.

The activation profile of Mac is thought to be important for host defenses against *Cryptococcus* (31, 35, 39, 41, 42) and other intracellular pathogens, including *Legionella* and mycobacteria (4, 10). Classically activated Mac (caMac) are thought to be important effector cells that eliminate *C. neoformans*, while aaMac are thought to serve as intracellular reservoirs of *C. neoformans* (13, 16, 35, 41). At the molecular level, these differences in microbicidal potential of caMac and aaMac are linked to differential upregulation of L-arginine-consuming enzymes inducible nitric oxide synthase (iNOS) and arginase (Arg1) (2, 12, 16, 41, 42). Studies of metabolic usage of L-arginine by the Arg1 and iNOS enzymes in Mac challenged with *C. neoformans* demonstrated that fungistasis correlates with nitric oxide (NO) production by Mac, while L-arginine consumption by Arg1 is nonfungicidal (14, 15).

Apart from the direct microbicidal effects, caMac and aaMac can differentially contribute to the inflammatory milieu. The caMac can produce acute-phase inflammatory cytokines (interleukin-1β [IL-1β], IL-12, and tumor necrosis factor alpha [TNF-α]) (27) and chemokines (such as macrophage inflammatory protein 1α [MIP-1α]/CCL3) (25, 27), which have been shown to be factors essential for generation of protective Th1 immunity (19, 21, 22, 34). In contrast, aaMac can produce mediators of chronic inflammation (such as transforming growth factor β [TGF-β]), chemokine receptor 4 ligands (TARC/CCL17, MDC/CCL22), lipid mediators (such as 12-hydroxyeicosatetraenoic acid [12-HETE] and 15-HETE), and chitinase family proteins (such as Ym1, Ym2, and Fizz1),

* Corresponding author. Mailing address: VA Ann Arbor Health System Research Service (11R), 2215 Fuller Rd., Ann Arbor, MI 48105. Phone: (734) 845-5238. Fax: (734) 845-3241. E-mail: olszewsm@umich.edu.

▽ Published ahead of print on 7 March 2011.

which can interfere with microbial clearance and/or promote pathology in the lungs (24, 25, 32, 35, 36, 40, 43).

One of the unanswered questions in this chronic ABPM model is how the changes in pulmonary cytokine environment over the course of infection affect the induction of aaMac versus caMac. Another important question is whether the manipulations of cytokine environment affect the fate of Mac activation during chronic ABPM and whether a mixed cytokine environment results in an intermediate Mac phenotype. The goal of this study was to dissect the effects of cytokine interplay on the fate of Mac activation by comparing expression levels of pulmonary cytokines and hallmarks of Mac activation in *C. neoformans*-infected WT, IL-4$^{-/-}$, and IFN-$\gamma^{-/-}$ mice. Furthermore, we sought to study Mac differentiation plasticity to see if an intermediate Mac activation phenotype can develop in a mixed cytokine environment.

MATERIALS AND METHODS

Mice. Female WT, IL-4$^{-/-}$, and IFN-$\gamma^{-/-}$ mice, all on a C57BL/6 genetic background (16 ± 2 g), were obtained from The Jackson Laboratory. Mice were 8 to 12 weeks of age at the time of infection. Mice were housed in sterile filter-top cages. Food and water were given *ad libitum*. The mice were maintained by the Unit for Laboratory Animal Medicine at University of Michigan (Ann Arbor, MI), in accordance with regulations approved by the University of Michigan Committee on the Use and Care of Animals (UCUCA).

***Cryptococcus neoformans*.** *C. neoformans* strain 24067 was obtained from the American Type Culture Collection. For infection, yeast cells were grown to stationary phase (48 to 72 h) at 34°C in Sabouraud dextrose broth (1% neopeptone, 2% dextrose; Difco, Detroit, MI) on a shaker. The cultures were then washed in nonpyrogenic saline (NPS), counted on a hemocytometer, and diluted to 3.3×10^5 CFU/ml in sterile nonpyrogenic saline.

Intratracheal inoculation of *C. neoformans*. Mice were anesthetized by intraperitoneal injection of ketamine (100 mg/kg of body weight; Fort Dodge Laboratories, Fort Dodge, IA) and xylazine (6.8 mg/kg; Lloyd Laboratories, Shenandoah, IA) and restrained on a small surgical board. A small incision was made through the skin over the trachea, and the underlying tissue was separated. A 1-ml tuberculin syringe filled with diluted *C. neoformans* culture, with the attached 30-gauge needle, was installed in a precision dispenser (Stepper; Tridak LLC, Torrington, CT). The needle was inserted into the trachea, and 30 μl of inoculum (10^4 cells) was dispensed into the lungs. The needle was removed, and the skin was closed with cyanoacrylate adhesive. The mice recovered with minimal visible trauma.

Bronchoalveolar lavage (BAL). Euthanized mice were lavaged after cannulation of the trachea with polyethylene tubing (PE50), which was attached to a 25-gauge needle on a tuberculin syringe. The lungs were lavaged twice with 1.0 ml of phosphate-buffered saline (PBS) containing 5 mM EDTA. The recovered fluid (1.6 to 1.8 ml total) was spun at 1,500 rpm to isolate the cell pellet for further analysis.

Lung leukocyte isolation. Individual lungs were excised, minced, and enzymatically digested for 30 min in 15 ml of digestion buffer (RPMI medium, 5% fetal calf serum [FCS], antibiotics, 1 mg/ml collagenase, and 30 μg/ml DNase). The cell suspension and undigested fragments were further dispersed by being drawn up and down 20 times through the bore of a 10-ml syringe. After erythrocyte lysis using NH_4Cl buffer (0.83% NH_4Cl, 0.1% $KHCO_3$, and 0.037% Na_2EDTA, pH 7.4), cells were washed, resuspended in RPMI medium, drawn up and down 20 times, filtered through a Nitex screen to remove debris, and centrifuged for 30 min at 2,000 × *g* in the presence of 20% Percoll (Sigma-Aldrich) to separate leukocytes from cell debris and epithelial cells. The isolated leukocytes were repelleted and resuspended in complete media. Total viable lung leukocyte numbers were assessed in the presence of trypan blue using a hemocytometer.

Mac separation for Mac/monocyte enrichment. The separation of monocytes and Mac on the basis of surface marker expression was done using magnetic cell sorting (MACS) as per manufacturer's instructions (Miltenyi Biotec GmbH). Briefly, isolated lung leukocytes were preincubated at 4°C for 20 min with biotin-conjugated anti-mouse CD11b monoclonal antibody (MAb) (PharMingen) added to 10^7 cells in labeling buffer. The cells were washed, further incubated with streptavidin microbeads (Miltenyi Biotec GmbH), and separated on a magnetic column (LS separation column). Cells were enriched up to 80% upon separation as determined by fluorescence-activated cell sorter (FACS) analysis (data not shown).

Histology. Lungs were fixed by inflation with 1 ml of 10% neutral buffered formalin, excised *en bloc*, and immersed in neutral buffered formalin. After paraffin embedding, 5-μm sections were cut and stained with mucicarmine (for *C. neoformans*) and counterstained with hematoxylin and eosin (H&E). Sections were analyzed with light microscopy, and microphotographs were taken using a DFX1200 digital microphotography system with ACT-1 software (Nikon Co., Tokyo, Japan).

RNA isolation and one-step RT PCR amplification. Lungs were harvested and homogenized in 3 ml of TRIzol reagent (Life Technologies, Inc., Gaithersburg, MD) in polypropylene tubes. Cells in suspension were spun down and directly resuspended in 1 ml Trizol. Samples were allowed to incubate at room temperature, and 200 μl chloroform per 1 ml Trizol was added to them. Samples were spun at 10,000 rpm for 15 min, aqueous phase was transferred into fresh tubes, and equal volumes of isopropanol were added. Samples were then allowed to sit at room temperature for 15 min and centrifuged again as described above. Pellets were washed with 1 ml of 80% ethanol and centrifuged. RNA was resuspended in diethyl pyrocarbonate (DEPC) water containing 1 μl/ml RNasin (Promega). The yield and purity of the RNA were determined spectrophotometrically at 260 and 280 nm. PCR amplification was set up with 1 μg RNA. The reaction mix was made using an Access reverse transcriptase PCR (RT PCR) system (Promega) that contained 25 units avian myeloblastosis virus (AMV) reverse transcriptase, 25 units *Tfl* DNA polymerase, 5 μl AMV/*Tfl* polymerase 5× reaction buffer, 0.2 mM deoxynucleoside triphosphate (dNTP), 2 μM forward and reverse primer, 1 mM $MgSO_4$, and nuclease-free water in a final volume of 25 μl per reaction. Reaction mix (15 μl) was added to RNA (10 μl) and amplified using the following parameters: pre-PCR step at 45°C for 45 min and 94°C for 2 min; cycling steps of denaturation at 94°C for 120 s, annealing at 58°C for 60 s, and elongation at 72°C for 90 s; and a final extension step at 68°C for 7 min. Forward and reverse primers used and product sizes of various genes amplified are listed in Table 1. After amplification, PCR products underwent electrophoresis on a 2% agarose gel containing 0.3 μg/ml ethidium bromide and a DNA ladder for the size comparison. Bands were visualized and photographed using a translucent UV source. The primer sequences and confirmation of specificity of the PCR products were described previously (2, 28, 34).

RT PCR. Semiquantitative RT PCR was performed on an ABI Prism 7000 thermocycler (Applied Biosystems) attached to a Dell Latitude laptop computer. Briefly, the reaction mixture contained 100 ng of cDNA, 12.5 μl of TaqMan 2× universal PCR master mix (Applied Biosystems and Roche), 250 nM probe, and forward and reverse primers at 300 nM in a final volume of 25 μl. For each time point, samples from individual mice ($n = 2$ or 3) were run in triplicate. The average cycle threshold (C_T) was determined for each group of animals from a given experiment. Relative gene expression was calculated using the comparative C_T method (11), which assesses the difference in gene expression between the gene of interest and an internal standard gene for each sample to generate the $\Delta\Delta C_T$. Relative gene expression was then determined by the formula $2^{-\Delta\Delta CT}$. The average for the IL-4$^{-/-}$ group was set to 1 for each independent experiment. Graphs are representative of 3 or more independent experiments for each gene of interest.

Immunohistochemical analysis of lung tissue and isolated Mac. Formalin-fixed, paraffin-embedded histological sections were used for immunohistochemical analysis of Mac. Sections were deparaffinized and rehydrated through a xylene-alcohol series to a final wash in PBS. The slides were microwaved in the presence of 10 mM citric acid (pH 6.0) for 15 min for antigen (Ag) retrieval. To quench endogenous peroxidase activity, samples were incubated with 3% H_2O_2 for 5 min. After the tissue was blocked with normal rabbit serum for 20 min, the sections were incubated with either rat isotype control antibody (Ab) or anti-Ym1/2 MAb generously provided by Shioko Kimura from NCI, Bethesda, MD (40). Following antibody incubation at 1:500 for 30 min at room temperature, slides were washed in buffer and stained with the biotinylated secondary antibody (rabbit anti-rat Ig) for another 30 min. Slides were incubated with Vectastain ABC Elite reagent (Vector Laboratories), developed using peroxidase substrate solution for 3 min, dehydrated, and mounted. Specimens were examined in a light microscope. CD11b-enriched cells were allowed to adhere to slides overnight at 37°C. Adherent cells were fixed with 10% formalin and permeabilized with 0.5% NP-40 solution for 15 min. Cells were then treated with 3% H_2O_2 for 5 min (to quench endogenous peroxidase activity) and stained with Ym1/2 Ab as described above. Numbers of Ym1/2-positive cells were counted under a microscope.

Bone marrow-derived Mac (BMM) cultures. Bone marrow cells were harvested from flushed marrow cavities of femurs and tibiae of uninfected mice under aseptic conditions and were cultured at 3×10^5 cells/ml (37°C and 5% CO_2) in L929 conditioned complete medium. After 7 days, the nonadherent cell

TABLE 1. List of primer sequences used for RT PCR

Target	Sense sequence (5′→3′)	Antisense sequence (5′→3′)	Band size (bp)
IFN-γ	CTACCTCAGACTCTTTGAAGTCT	CAGCGACTCCTTTTCCGCTT	242
TNF-α	CCTGTAGCCCACGTCGTAGC	AGCAATGACTCCAAAGTAGACC	431
IL-4	CTGACGGCACAGAGCTATTGA	TATGCGAAGCACCTTGGAAGC	250
IL-5	GAGCACAGTGGTGAAAGAGACCTT	ATGACAGGTTTTGGAATAGCATTT	201
IL-13	GCCAGCCCACAGTTCTACAGC	GAGATGTTGCTCAGCTCCTCA	181
iNOS	TTTGCTTCCATGCTAATGCGAAAG	GCTCTGTTGAGGTCTAAAGGCTCCG	600
Arginase	CAGAAGAATGGAAGAGTCAG	CAGATATGCAGGGAGTCACC	249
Fizz1	GGTCCCAGTGCATATGGATGAGACCATAGA	CACCTCTTCACTCGAGGGACAGTTGGCAGC	348
CCL22	TCTGATGCAGGTCCCTATGGT	TTATGGAGTAGCTTCTTCAC	205
CXCL9	GAGCACAGTGGTGAAAGAGACCTT	ATGACAGGTTTTGGAATAGCATTT	275
CXCL10	GCCAGCCCACAGTTCTACAGC	GAGATGTTGCTCAGCTCCTCA	521
MGL2	GATAACTGGCATGGACATATG	TTTCTAATCACCATAACACATTC	300
12/15-LOX	CAGCTGGATTGGTTCTACTG	CTCTGAACTTCTTCAGCACAG	243
β-Actin	TGGAATCCTGTGGCATCCATGAAAC	TAAAACGCAGCTCAGTAACAGTCCG	348

populations were discarded, and the adherent cells were removed by cell scraping following incubation on ice for 20 min in PBS containing 1 mM EDTA. Cells were counted, transferred to 8-well glass Labtek tissue culture plates at a cell density of 1×10^5 cells/well, and incubated for an additional 24 h at 37°C and 5% CO_2 in media alone or with recombinant mouse cytokines from Peprotech Inc. (Rocky Hill, NJ): IFN-γ (100 ng/ml), IL-4 (20 ng/ml), or a combination of both cytokines. Following the incubation, cells were harvested for RNA isolation or immunofluorescence staining.

Immunofluorescence analysis of intracellular proteins in BMM. Cells were fixed, permeabilized with 0.1% Triton X-100, and blocked with PBS-2% bovine serum albumin (BSA). Wells were incubated sequentially with anti-iNOS fluorescein isothiocyanate (FITC)-conjugated antibodies, anti-Arg1 Alexa Fluor 546 phalloidin (Imgenex, San Diego, CA), and DAPI (4′,6-diamidino-2-phenylindole) (to stain cell nuclei) and analyzed with a Zeiss LSM510 confocal microscope.

Statistical analysis. All values are means ± standard errors of the means (SEM), unless otherwise indicated. Differences between two means were evaluated using the Student *t* test (assuming equal variance as dictated by the F test), with a P value of <0.05 considered to be statistically significant at a single comparison. Bonferroni's adjustment for multiple comparisons was used to determine significance whenever multiple groups were compared.

RESULTS

Effect of IL-4 and IFN-γ deletion on clearance pattern and pulmonary cytokine expression in *C. neoformans*-infected lungs. To further the understanding of cytokine interplay during chronic *C. neoformans* infection and to determine how IL-4 and IFN-γ regulate other cytokines in this model, kinetics of pulmonary cytokine expression was evaluated in WT, IL-$4^{-/-}$, and IFN-$\gamma^{-/-}$ mice. Cytokine expression in whole lung mRNA was evaluated by RT PCR at 2, 3, and 5 weeks postinfection (wpi). Although WT mice showed a Th2 cytokine bias at 2 and 3 wpi, cytokine analysis revealed increases in the levels of IFN-γ and TNF-α between 3 and 5 wpi and a decline of IL-4 at 5 wpi (Fig. 1). IL-4 deletion resulted in earlier and stronger induction of IFN-γ and a corresponding increase in TNF-α expression, suggesting that IFN-γ promotes TNF-α production during chronic fungal infection. Consistently, TNF-α was not induced in IFN-$\gamma^{-/-}$ mice throughout all analyzed time points. Levels of expression of IL-5 were similar in all three infected groups of mice, suggesting that pulmonary IL-5 expression was regulated independently from IL-4 and IFN-γ in this model. Likewise, IL-13 was expressed in all infected groups at 2 and 3 wpi. At week 5, however, IL-13 expression was more pronounced in IFN-$\gamma^{-/-}$ mice than in WT and IL-$4^{-/-}$ mice. Concurrently with cytokine analysis, we confirmed chronic infection with a relatively constant fungal load in WT mice, improved clearance in IL-$4^{-/-}$ mice, and an increased fungal load in IFN-$\gamma^{-/-}$ mice infected with *C. neoformans* (not shown), as reported previously (2, 18). These results demonstrate (i) an inverse correlation between induction of IL-4 and IFN-γ in WT mice, (ii) an enhanced expression of Th1 cytokines in the absence of IL-4, (iii) a positive correlation of TNF-α and IFN-γ, and (iv) a correspondence between the pulmonary fungal burdens and the differences in cytokine levels as well as the reported role of these cytokines in cryptococcal infections. Together, these results illustrate that multilevel regulation of Th1 and Th2 cytokines modulates immune responses and fungal control during ABPM/chronic fungal infection in the lungs.

Role of IL-4 and IFN-γ in regulating expression of iNOS and Arg1 enzymes. We next compared the kinetics of expression of L-arginine-consuming enzymes by RT PCR (Fig. 2). iNOS is a source of fungicidal NO, and Arg1 is responsible for

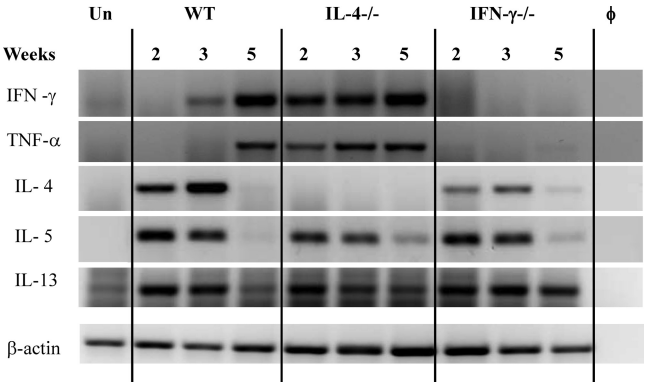

FIG. 1. Effect of IL-4 and IFN-γ deletion on cytokine expression in *C. neoformans*-infected lungs. Total lung RNA was isolated from uninfected and *C. neoformans*-infected mice at 2, 3, and 5 wpi. RT PCR was performed for selected cytokines, and electrophoresis of PCR products was performed in a 2% agarose gel. Photographs show bands of the predicted sizes. ϕ, no-RNA control; Un, uninfected WT mice. Each lane is representative of 3 to 5 mice/group/time point. Baseline expression levels of cytokines were similar in uninfected lungs from WT, IL-$4^{-/-}$, and IFN-$\gamma^{-/-}$ mice.

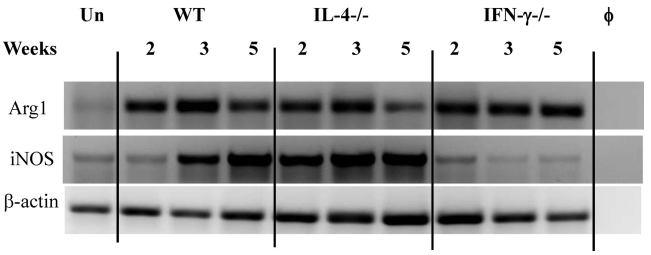

FIG. 2. Effect of IL-4 and IFN-γ deletion on the kinetics of iNOS and arginase mRNA expression during *C. neoformans* infection. RNA from WT, IL-$4^{-/-}$, and IFN-$\gamma^{-/-}$ mice was isolated and analyzed as described in the legend for Fig. 1. Photographs show bands of the predicted sizes for each PCR product. ϕ, no-RNA control; Un, uninfected WT mice. Each lane is representative of 3 to 5 mice/group/time point.

nonfungicidal L-arginine consumption. Arg1 was induced following infection in all three groups of mice, and it declined modestly in the WT mice at 5 wpi. This decline in Arg1 expression was not observed in IFN-$\gamma^{-/-}$ mice, but it was more pronounced in the IL-$4^{-/-}$ mice at 5 wpi (Fig. 2). WT mice showed a gradual increase in iNOS expression throughout the observed time course of infection. In contrast, IL-$4^{-/-}$ mice expressed high levels of iNOS at all time points, whereas IFN-$\gamma^{-/-}$ mice expressed low levels of iNOS similar to that seen in the uninfected control. This pattern of iNOS expression follows the IFN-γ and TNF-α expression pattern in the infected lungs (Fig. 1). A higher iNOS-arginase ratio in the IL-$4^{-/-}$ mice than in the WT or IFN-$\gamma^{-/-}$ mice is consistent with improved fungal clearance, suggesting that the IFN-γ/IL-4 balance modulates cryptococcal clearance by regulating the iNOS/Arg1 ratio in the infected lungs.

Effect of IL-4 and IFN-γ deletion on the development of ABPM pathology following *C. neoformans* infection. Next, we analyzed lung pathology in tissue sections from *C. neoformans*-infected WT, IL-$4^{-/-}$, and IFN-$\gamma^{-/-}$ mice at 5 wpi. The WT mice developed extensive ABPM pathology, with large areas of consolidated inflammation in the lungs and a few open air spaces (Fig. 3A). In contrast, IL-$4^{-/-}$ mice had predominantly open air spaces, similarly to the result seen in the lungs of uninfected mice, with a few well-defined areas of dense inflammatory infiltrates in bronchovascular regions (Fig. 3B). In IFN-$\gamma^{-/-}$ mice, severe inflammation displaced virtually all normal lung tissue, with areas of cryptococcal expansion visible even in the low-power images (Fig. 3C). High-power images revealed a mixed inflammatory infiltrate in WT mice, with a predominance of Mac, including multinucleated giant cells and intracellular yeast cells (Fig. 3D). In contrast, IL-$4^{-/-}$ mice had infiltrates composed of small mononuclear phagocytes mixed with lymphocytes, and there was no intracellular *C. neoformans* in these cells (Fig. 3E), consistent with a Th1-type cellular infiltrate. The inflammatory response in IFN-$\gamma^{-/-}$ mice resembled that in the WT mice, with even greater numbers of organisms residing within Mac and a higher proportion of granulocytes. Furthermore, Mac in IFN-$\gamma^{-/-}$ mice contained eosinophilic crystals, previously shown to be composed of two related chitinase-like proteins, Ym1 and Ym2 (2, 40), which are markers of aaMac (Fig. 3F).

Apart from the presence of inflammatory cells, hypertrophy of airway epithelial cells and thickening of the basement membrane were noted in the WT mice (Fig. 3G). These histologic changes of epithelium were absent in IL-$4^{-/-}$ mice (Fig. 3H) but were even more pronounced in IFN-$\gamma^{-/-}$ mice. Epithelial cells from IFN-$\gamma^{-/-}$ mice contained pink-staining "hyaline inclusions," displacing cell nuclei toward the basement membrane as well as disrupting the epithelial lining (Fig. 3I). IFN-$\gamma^{-/-}$ mice developed large cryptococcomas, a collection of organisms with halos of mucoid capsular material and a few inflammatory cells (Fig. 3J). The Ym1/2 crystals seen within Mac were also found occasionally within the airway lumen of IFN-$\gamma^{-/-}$ mice (Fig. 3K) but not that of the WT or IL-$4^{-/-}$ mice. Furthermore, evidence of secretion of eosinophilic inclusions (hyaline bodies) from the epithelial cells into the airway lumen was observed in IFN-$\gamma^{-/-}$ mice (Fig. 3K). These results demonstrate that IL-4 promotes the development of severe pathological symptoms in ABPM/chronic fungal infection in the lungs, while IFN-γ ameliorates but does not prevent ABPM pathology.

Role of cytokines in regulating Ym1/2 production in the lungs of uninfected and *C. neoformans*-infected mice. To examine the role of IL-4 and IFN-γ in Ym1/2 production by Mac *in vivo*, lung sections from *C. neoformans*-infected WT, IL-$4^{-/-}$, and IFN-$\gamma^{-/-}$ mice were stained with Ym1/2 Ab (40). We first determined whether the deletion of IL-4 or IFN-γ affected the basal Ym1/2 protein level in alveolar Mac. Lung sections from uninfected WT, IL-$4^{-/-}$, and IFN-$\gamma^{-/-}$ mice were immunohistochemically stained with Ym1/2 MAb. Ym1/2-positive Mac were equally abundant in the lungs of all three uninfected strains of mice (Fig. 4A to C), indicating that basal Ym1/2 production occurs in resident alveolar Mac and is independent of IL-4 and IFN-γ regulation. The density of Ym1/2-positive cells increased dramatically at 3 wpi in WT and IFN-$\gamma^{-/-}$ mice and to a much lesser extent in IL-$4^{-/-}$ mice (Fig. 4D to F). At 5 wpi, WT mice maintained a relatively large number of Ym1/2-positive cells in the lungs (Fig. 4G). In contrast, the lungs of IL-$4^{-/-}$ mice had minimal numbers of Ym1/2-positive cells at 5 wpi, and this Ym1/2 staining resembled that of the uninfected mice (Fig. 4H). An opposite trend in pulmonary expression of Ym1/2 protein was observed in IFN-$\gamma^{-/-}$ mice. Increased areas of consolidated cells with strong Ym1/2 production were noted in the IFN-$\gamma^{-/-}$ lungs at 5 wpi (Fig. 4I). All Ym1/2-positive cells had a foamy Mac or multinucleated giant cell morphology, and formation of Ym1/2 crystals occurred along the yeast cell walls (Fig. 4J to O). In contrast, Mac in IL-$4^{-/-}$ mice showed weak and diffused Ym1/2 staining and largely "empty" vacuoles consistent with degraded organisms. At 5 wpi, crystal formation was much greater in IFN-$\gamma^{-/-}$ mice than in WT mice. These results suggest that IL-4 and IFN-γ have opposite stimulatory and counterregulatory effects on Ym1/2 production by Mac in *C. neoformans*-infected lungs.

Effect of IL-4 and IFN-γ on accumulation of Ym1/2-positive and -negative Mac in *C. neoformans*-infected lungs. Our next goal was to determine if the differences seen in Ym1/2 accumulation in histological sections were due to the changes in Mac numbers or differential expression of Ym1/2 proteins by these cells. Our previous studies demonstrated that Mac and monocytes recruited to the lungs during *C. neoformans* infection express CD11b. Lung leukocytes were isolated from the infected mice and enriched for CD11b by MACS separation.

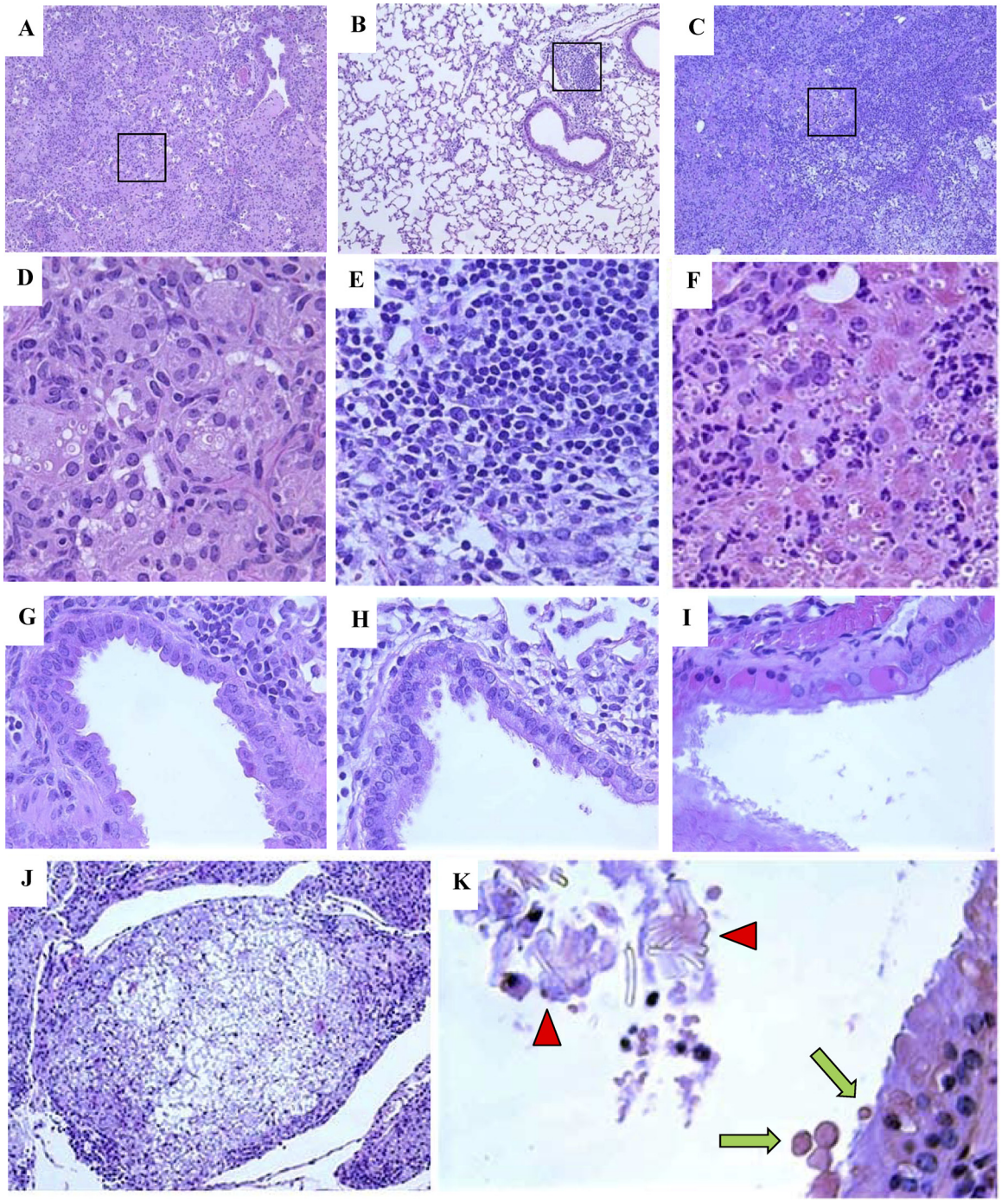

FIG. 3. Effect of IL-4 and IFN-γ deletion on ABPM pathology in *C. neoformans*-infected lungs. Photomicrographs are H&E-stained sections of *C. neoformans*-infected lungs from WT (A, D, and G), IL-$4^{-/-}$ (B, E, and H), and IFN-$\gamma^{-/-}$ (C, F, and I to K) mice at 5 wpi. Low-power images (A, B, and C) demonstrate differences in the extent of inflammatory responses and consolidation of lung tissue (10× objective). High-power images (D, E, and F) of the boxed areas demonstrate cellular composition and differences in Mac morphology (40× objective). Note the absence of microbe in IL-$4^{-/-}$ lungs and the increased microbial presence and accumulation of eosinophilic deposits in the Mac in IFN-$\gamma^{-/-}$ lungs. High-power images of airway sections (G, H, and I) demonstrate differences in airway epithelium. Note the presence of eosinophilic inclusions in the epithelial cells of IFN-$\gamma^{-/-}$ mice (I). Severe pulmonary pathology in IFN-$\gamma^{-/-}$ lungs is highlighted by the formation of cryptococcomas (J, 10× objective), the presence of eosinophilic crystals in the airway lumen (K, 40× objective, red arrowheads), and the secretion of eosinophilic inclusions in the airway lumen, or hyalinosis (K, green arrows).

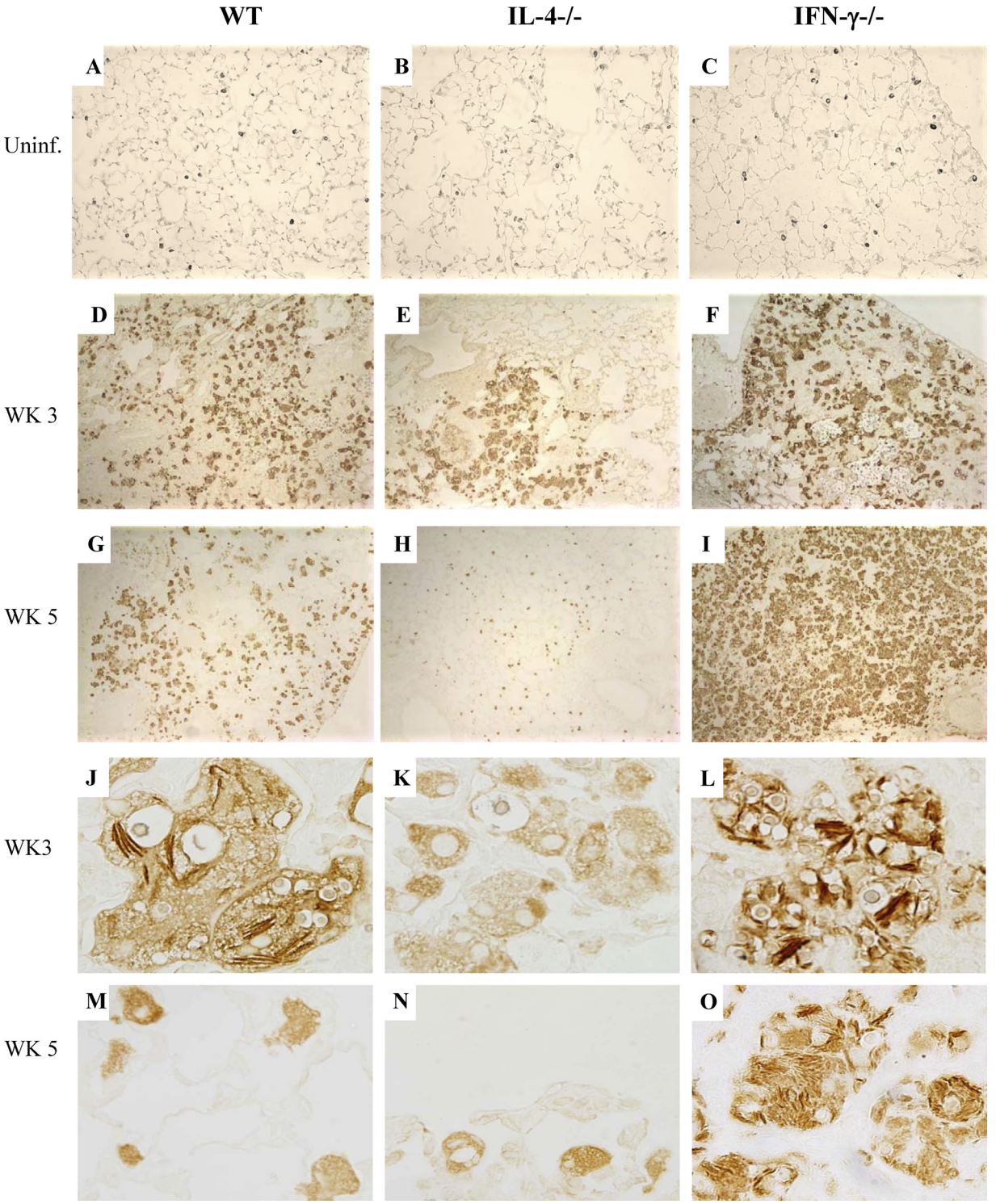

FIG. 4. Effects of IFN-γ and IL-4 deletion on regulation of Ym1/2 production by Mac in uninfected and *C. neoformans*-infected lungs. Sections of uninfected WT, IL-4$^{-/-}$, and IFN-γ$^{-/-}$ mouse lungs (A, B, and C) and *C. neoformans*-infected lungs (D to O) were immunostained with anti-Ym1/2 antibody and developed with a peroxidase-linked detection system. Sections shown in panels A to F and J to L were photographed using a 10× objective, while those in panels G to I and M to O were photographed using a 100× objective. Note that the basal level of Ym1/2 production by Mac in the uninfected lungs was not affected by IL-4 or IFN-γ deletion; however, accumulation of Ym1/2-positive Mac and intracellular Ym1/2 crystal deposition are ablated in IL-4$^{-/-}$ and augmented in IFN-γ$^{-/-}$ infected lungs.

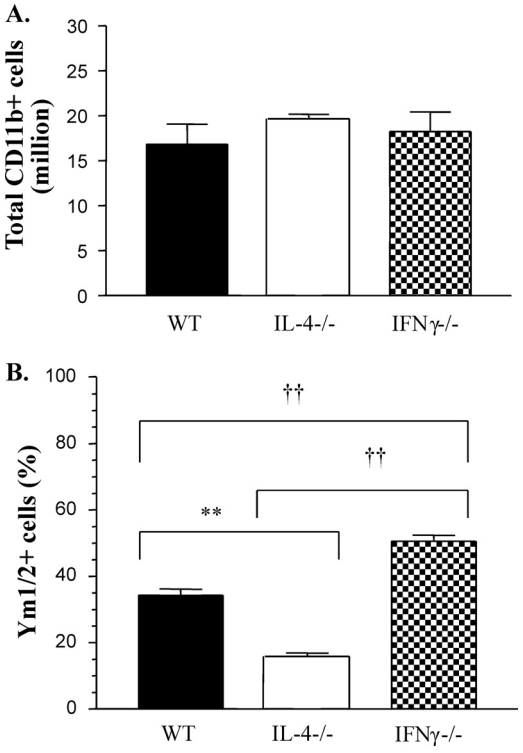

FIG. 5. Effects of IFN-γ and IL-4 deletion on numbers of Ym1/2-expressing CD11b$^+$ cells in *C. neoformans*-infected lungs. (A) CD11b-expressing cells were isolated from *C. neoformans*-infected WT, IL-4$^{-/-}$, and IFN-γ$^{-/-}$ mice (3 wpi) by MACS separation and counted under a microscope. The data are means from 3 independent experiments, with ≥3 mice/group/experiment. (B) CD11b-selected cells were stained with Ym1/2 Ab to enumerate Ym1/2-positive and -negative cells. Approximately 100 cells were counted in 10 different fields on a slide. **, $P < 0.005$ for the IL-4$^{-/-}$ group compared to the WT group; ††, $P < 0.005$ for the IL-4$^{-/-}$ group compared to the IFN-γ$^{-/-}$ group. Note that the total number of CD11b-selected cells was not affected by IL-4 or IFN-γ deletion but that there was a strong effect on the numbers of cell staining positive for Ym1/2.

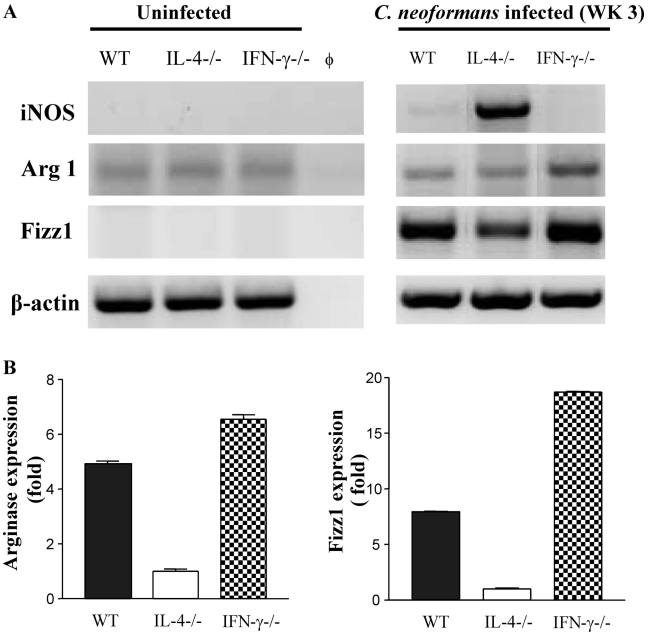

FIG. 6. Effects of IFN-γ and IL-4 deletion on the expression of selected caMac and aaMac genes by Mac from uninfected and *C. neoformans*-infected mice. RNA from enriched Mac isolates was analyzed at 3 wpi. (A) RT PCR mRNA analysis of RNA from iNOS, Arg1, and Fizz1 was performed as described in the legend for Fig. 1. The band photographs are representative of 3 independent experiments. (B) RNA from each sample was subjected to semiquantitative RT PCR analysis for Arg1 and Fizz1, and expression was normalized to GAPDH (glyceraldehyde-3-phosphate dehydrogenase) housekeeping gene expression within each sample. The average relative expression of each gene in IL-4$^{-/-}$ cells in each independent experiment was used to calculate the relative expression ratios for WT and IFN-γ$^{-/-}$ cells. The graph is representative of 3 or more experiments, where each sample was run in triplicate ($n = 3$ mice/group).

Total numbers of monocytes/Mac (CD11b$^+$ cells) isolated from WT, IL-4$^{-/-}$, and IFN-γ$^{-/-}$ mice were not significantly different at week 3 (Fig. 5A), suggesting that differences seen in Ym1/2 crystal accumulation were not due to differences in Mac numbers.

Subsequently, we compared the proportions of Ym1/2-producing Mac in the lungs of these animals. The CD11b-enriched cells were fixed onto a glass slide, immunostained with Ym1/2 MAb, and counted under a microscope. Approximately 35% of Mac from the WT mice were positive for Ym1/2, while significantly lower (15%) and significantly higher (50%) percentages of Ym1/2-positive cells were found in Mac isolated from IL-4$^{-/-}$ and IFN-γ$^{-/-}$ mice, respectively (Fig. 5B). Together, these results demonstrate that IL-4 enhanced while IFN-γ decreased Ym1/2 production by pulmonary Mac.

Role of IL-4 and IFN-γ in polarization of Mac during fungal infection. We next analyzed pulmonary Mac polarization in uninfected and infected mice at 3 wpi. Cells were collected from BAL fluid of uninfected WT, IL-4$^{-/-}$, and IFN-γ$^{-/-}$ mice, and RNA was extracted for RT-PCR analysis. Expression of caMac marker iNOS as well as aaMac markers Arg1 and Fizz1 was determined. The uninfected alveolar Mac did not expressed iNOS or Fizz1, but low levels of Arg1 mRNA were detected in all three groups (Fig. 6A). No differences in the baseline levels of Arg1 expression were observed among the uninfected WT, IL-4$^{-/-}$, and IFN-γ$^{-/-}$ Mac groups (Fig. 6A), indicating that IL-4 and IFN-γ do not regulate basal expression of Arg1 in alveolar Mac.

The iNOS and Arg1 expression data from the enriched inflammatory (CD11b$^+$) Mac populations isolated from infected lungs at 3 wpi were further examined (Fig. 6). The outcomes confirmed the findings from total lung RNA (Fig. 2). iNOS expression strongly prevailed over Arg1 expression in Mac from the infected IL-4$^{-/-}$ mice, and an opposite pattern of iNOS-Arg1 proportions was observed in Mac from IFN-γ$^{-/-}$ mice (Fig. 6A). Interestingly, Fizz1 mRNA expression in inflammatory Mac was significantly upregulated in all groups compared to that in resident Mac; however, Fizz1 was most significantly induced in Mac from IFN-γ$^{-/-}$ mice and least significantly induced in Mac from IL-4$^{-/-}$ mice at 3 wpi (Fig. 6A and B). As for the other caMac/aaMac markers, WT mice showed an intermediate Fizz1 expression pattern compared to that for their IL-4$^{-/-}$ and IFN-γ$^{-/-}$ counterparts. Together, these data further strengthen our observation that resident pulmonary Mac in C57BL/6 WT mice show low levels of ex-

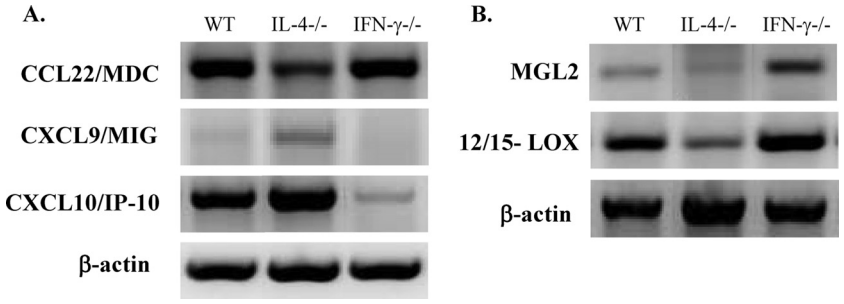

FIG. 7. Effects of IFN-γ and IL-4 deletion on the expression of aaMac- and caMac-specific markers by Mac from *C. neoformans*-infected mice. CD11b-selected cell isolates were analyzed for mRNA expression of chemokines (A) or MGL2 and 12/15-LOX (B) at 3 wpi. Photographs show the bands of predicted sizes and are representative of 3 or more independent experiments.

pression of selected aaMac genes independent of IL-4/IFN-γ; however, Mac recruited during cryptococcal infection are strongly polarized by IL-4 and IFN-γ to display aaMac and caMac phenotypes, respectively.

Assessment of additional caMac versus aaMac polarization markers relevant to chronic inflammatory process in *C. neoformans*-infected WT, IL-4$^{-/-}$, and IFN-γ$^{-/-}$ mice. Expression of chemokines known to be differentially expressed in caMac and aaMac was assessed at 3 wpi to further dissect Mac phenotypes. The aaMac were shown to upregulate MDC/CCL22, which contributes to Th2 inflammation/pathology in pulmonary *Schistosoma* antigen challenge (23) and in allergic aspergillosis (17). Mac from IFN-γ$^{-/-}$ mice showed the highest expression of CCL22, whereas Mac from IL-4$^{-/-}$ mice expressed the lowest level of CCL22 (Fig. 7A), consistent with the extent of Th2 pathology in each group (Fig. 3). We next analyzed MIG/CXCL9 and IP-10/CXCL10, which are expressed by caMac and implicated in protective T-cell-mediated responses and pulmonary accumulation of Th1 cells (26, 27, 33). The most pronounced expression of CXCL9 and CXCL10 was found in IL-4$^{-/-}$ Mac, while in IFN-γ$^{-/-}$Mac, expression of these chemokines was either minimal or undetectable (Fig. 7A). WT mice expressed chemokines that are characteristic of both caMac and aaMac, indicating the development of a mixed or intermediate Mac polarization phenotype.

Two other markers of aaMac are implicated in pathology of chronic inflammation. Mac galactose C-type lectin (MGL) and 12/15-lipoxygenase (12/15-LOX) enzyme have been shown to be upregulated in aaMac (5, 37). At 3 wpi, both MGL2 and 12/15-LOX were expressed at high levels in Mac from WT and IFN-γ$^{-/-}$ mice, compared to that seen in Mac from IL-4$^{-/-}$ mice (Fig. 7B). Together, these results explain differences in the types of pathologies observed in the infected WT, IL-4$^{-/-}$, and IFN-γ$^{-/-}$ mice, confirming the development of aaMac in IFN-γ$^{-/-}$ mice, caMac in IL-4$^{-/-}$ mice, and both caMac and aaMac and/or cells that possess features of both caMac and aaMac in WT mice.

Role of interplay between IL-4 and IFN-γ in regulating Mac polarization. Our analysis of aaMac and caMac gene expression indicated the development of a mixed or intermediate macrophage polarization phenotype when both IL-4 and IFN-γ were induced in the infected lungs. Our next goal was to evaluate whether Mac exposed to both cytokines separate into subgroups displaying either aaMac or caMac characteristics or, alternatively, display an intermediate activation phenotype. We used *in vitro* cultures of BMM from the WT mice cultured for 24 h in media alone or with IFN-γ, IL-4, or both. Expression of iNOS and Arg1 was evaluated at the mRNA and protein levels. The BMM cultured in media alone showed a slight caMac bias (Fig. 8A), i.e., low-level expression of iNOS and undetectable levels of Arg1. However, IFN-γ treatment dramatically upregulated iNOS expression, while IL-4 treatment resulted in a strong induction of Arg1. The combined cytokine treatment resulted in a strong induction of both Arg1 and iNOS within the 24-h period (Fig. 8A). Immunofluorescence studies revealed that the protein expression pattern mirrored the RNA expression data, demonstrating strong iNOS induction in IFN-γ-treated BMM (Fig. 8B, green) and strong induction of Arg1 in IL-4-treated BMM (Fig. 8B, red). Notably, BMM treated with a combination of IL-4 and IFN-γ demonstrated strong coinduction of both Arg1 and iNOS within the same cells. The vast majority of Mac cotreated with IL-4 and IFN-γ displayed yellow florescence resulting from a merge of double-positive staining for both Arg1 and iNOS proteins, providing evidence for intermediately activated Mac. Thus, Mac can rapidly assume the aaMac or caMac phenotype when treated with either IL-4 or IFN-γ. Most importantly, they display an "intermediate activation" phenotype, with strong expression of both caMac and aaMac genes within individual cells, when concurrently stimulated with both of these cytokines.

DISCUSSION

The goal of this paper was to dissect the effects of cytokine interplay on the establishment of chronic fungal infection, development of lung pathology, and fate of Mac polarization in the lungs during *C. neoformans* infection. Our study demonstrates that (i) cytokine expression in the chronic ABPM model is not permanently Th2 biased but changes dynamically over time, (ii) the balance between Th1 and Th2 cytokines supports chronic infection, chronic inflammation, and the development of ABPM pathology, (iii) IL-4 and IFN-γ play a critical role in the fate of Mac activation in the setting of an ABPM response, and (iv) the effects of these cytokines on Mac can be additive, resulting in an intermediate aaMac/caMac phenotype.

In contrast to a "fixed" view of the immune polarization paradigm, our data show that cytokine expression in the chronic ABPM model is not permanently biased. Our previous studies documented that pathological symptoms in *C. neofor-*

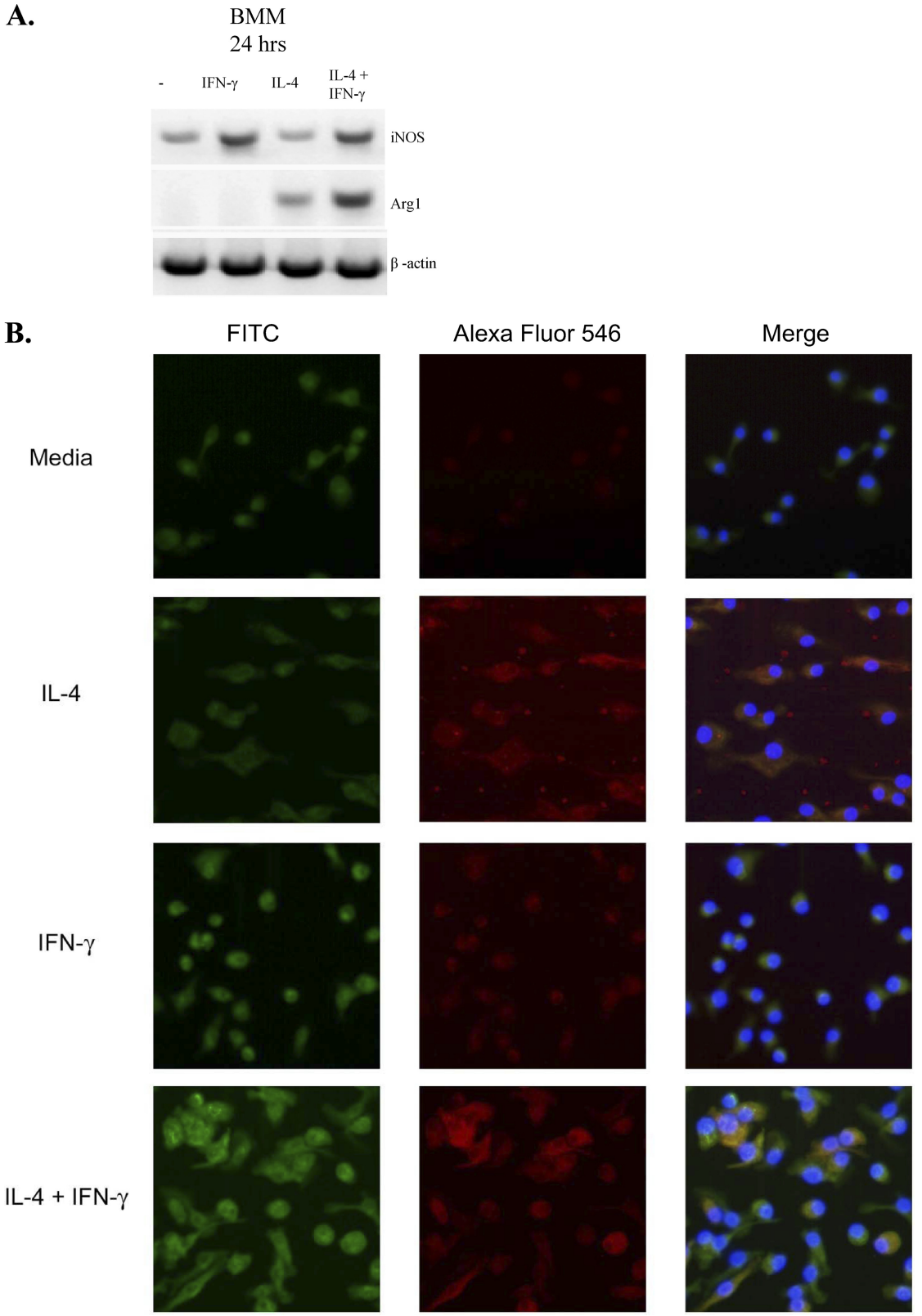

FIG. 8. Effects of IFN-γ and IL-4 on induction of iNOS2 and Arg1 in BMM. BMM from WT mice were precultured and isolated as described in Materials and Methods and transferred to 8-well glass Labtek tissue culture plates at a cell density of 1×10^5 cells/well for 24 h at 37°C and 5% CO_2 in media alone or with recombinant mouse IFN-γ, IL-4, or a combination of both cytokines. (A) RNA from these cells was collected and analyzed by RT PCR. (B) Cells were fixed, permeabilized, incubated sequentially with anti-iNOS FITC-conjugated antibodies, anti-Arg1 Alexa Fluor 546 phalloidin (Imgenex, San Diego, CA), and DAPI (to stain cell nuclei), and analyzed with a Zeiss LSM510 confocal microscope. Note the red Arg1 staining in IL-4-treated BMM, the green iNOS staining in IFN-γ-treated BMM, and the ARG1/iNOS double-positive staining in BMM treated with a combination of IL-4/IFN-γ. The individual green- and red-channel pictures are presented in the left and middle columns, respectively; the merged images are presented in the right column.

mans-infected C57BL/6 WT mice were related to a Th2 bias of the immune response (6, 7, 18); however, the role of IFN-γ was also demonstrated in this model (2). This motivated our kinetic analysis of the major Th polarizing cytokines at different time points of the adaptive immune response. Following the strong induction of Th2 cytokines in the lungs of WT mice at 2 and 3 wpi, a considerable increase in Th1 cytokines occurred at 5 wpi (Fig. 1). This unexpected increase in Th1 cytokines was accompanied by a decrease in Th2 cytokines, indicating that the immune system after an initial Th2 response is capable of a compensatory response that resembles (or is) a Th1 response. Interestingly, the compensatory changes in the cytokine profile are insufficient to support effective *C. neoformans* clearance. This indicates that the early induction of Th2 cytokines leads to the establishment of chronic disease and that, once this pathological pathway is in place, even the subsequent increases in IFN-γ and TNF-α cannot resolve this chronic infection. The mechanism of an "early/transient" Th2 response leading to chronic inflammation is likely involved not only in ABPM but also in other persistent infections. The chronic presence of microbe and absence of clearance are frequently associated with a perturbed immune response characterized by a mixed cytokine profile rather than with a "pure" Th2 immunity (3, 8, 19, 29, 38). Our data from the IL-4$^{-/-}$ and IFN-γ$^{-/-}$ infection models further support this view of complex cytokine regulation in chronic fungal infection. Generation of the early Th1-biased response in IL-4$^{-/-}$ mice and sustained Th1 cytokine production explain the robust clearance of infection and the absence of the detrimental lung pathology (albeit, IL-5 and IL-13 are still induced). The deletion of IFN-γ results in a more severe infection but does not result in a greater induction of IL-4 or IL-5, suggesting that decreasing IL-4 or IL-5 production is not a mechanism by which IFN-γ benefits the host in this model. In contrast, IFN-γ deletion abolishes TNF-α induction and enhances expression of IL-13 at the later time point, indicating that IFN-γ promotes late TNF-α production and acts as a negative regulator of IL-13. In summary, our cytokine data demonstrate that cytokine expression in the chronic ABPM model is not permanently fixed but changes dynamically over time. This mixed cytokine environment supports chronic infection, chronic inflammation, and ABPM pathology.

In terms of the role of IL-4/IFN-γ balance in the development of pulmonary pathology, IFN-γ$^{-/-}$ mice displayed more-severe lesions than the other mouse strains. Some pathological lesions found in these mice represent a quantitative increase of pathological features seen in the WT mice, including increased inflammation and consolidation of pulmonary tissue, formation of Ym1/2 crystals by Mac, and increased microbial burden. In addition, we observed a formation of cryptococcomas, densely packed organisms "suspended" in a thick capsular material with a few inflammatory cells in their peripheral zones (Fig. 3J), and hyalinosis, an eosinophilic cytoplasmic degeneration of airway epithelial cells (Fig. 3K). Furthermore, hypertrophy of epithelial cells, disruption of lining, and thickening of the basement membrane were noted in these mice (Fig. 3I). The disruption of airway epithelium in allergic airway diseases, such as asthma, is thought to be an important step perpetuating the cascade of allergic immune responses. Thus, IFN-γ not only limits fungal growth and Ym1/2 crystal formation by Mac but also ameliorates detrimental airway pathology in the setting of ABPM.

Our study also generated data important for understanding how Mac activation may change in the course of chronic fungal infection/ABPM. Rigorous analysis of aaMac versus caMac markers in the cells from infected WT, IL-4$^{-/-}$, and IFN-γ$^{-/-}$ mice illustrates that IL-4 and IFN-γ are the major factors driving the elements of alternative and classical activation of Mac, respectively (Fig. 4 to 7). Although levels of accumulation of CD11b-positive Mac/monocytes are equivalent in the lungs of infected WT, IL-4$^{-/-}$, and IFN-γ$^{-/-}$ mice (Fig. 5A), the aaMac versus caMac gene/protein expression profiles are different. Our *in vivo* findings document that IL-4 and IFN-γ play the major role in Mac polarization in this model, with IL-4 acting as an enhancer of aaMac gene expression and IFN-γ acting as a restrictor of aaMac gene expression and an enhancer of caMac genes. The differences in Mac polarization profile in the infected WT, IL-4$^{-/-}$, and IFN-γ$^{-/-}$ mice correspond with the differences in microbial clearance rate and development of pulmonary pathologies. The differential iNOS-arginase ratios in Mac from IL-4$^{-/-}$ and IFN-γ$^{-/-}$ mice are not only an indicator of differential caMac versus aaMac polarization status in these mice but also provide a good explanation for the opposite trends in fungal clearance from the lungs. The "gradation" iNOS-arginase ratios in the lungs of IL-4$^{-/-}$, WT, and IFN-γ$^{-/-}$ mice correlate with the respective levels of pulmonary clearance/growth of *C. neoformans*, supporting the notion that the ratio of iNOS/Arg1 is an important determinant of the *C. neoformans* clearance by Mac (1, 2, 12, 14–16, 41, 42).

In terms of Mac activation and the pathological outcomes, our data also suggest that alternative activation contributes to the development of pathological lesions. Apart from the visible harboring of *C. neoformans* by aaMac, documented by the enhanced presence of intracellular organisms in cells strongly expressing aaMac marker Ym1/2 (Fig. 4J to O), we found several mediators of chronic inflammation. Lipid mediators, such as those produced by 12/15-lipoxygenase and CCL22/MDC, were either directly implicated or associated (through the chronic recruitment of leukocytes) with airway pathology/remodeling, epithelial injury, and epithelial metaplasia (23, 24, 35). The chitinases, such as Ym1/2 and acidic mammalian chitinase (AMCase), have been also associated with epithelial injury and lung pathology (32, 40, 43). The induction of these aaMac products correlates with the level of lung pathology in the compared groups of infected mice.

In addition to the major opposing roles of IL-4 and IFN-γ in aaMac/caMac gene expression, our data suggest that other factors may contribute to the Mac phenotype. First, the alveolar Mac, which are the predominant leukocyte in the uninfected alveolar space, demonstrate some features of aaMac but not caMac (constitutive expression of Ym1/2 protein and low level of Arg1 mRNA but not iNOS) (Fig. 4 and 6). This constitutive Ym1/2 and Arg1 expression in the lungs is independent of IL-4 and IFN-γ, suggesting that other factors produced in the uninfected lungs are responsible for the low-level induction of aaMac genes. Second, the kinetic comparison of aaMac and caMac markers with the cytokine expression profiles in the infected lungs provides a clue about the possible involvement of other cytokines apart from IL-4 and IFN-γ.

The decreases in the numbers of Ym1/2-producing cells and Arg1 expression that are observed in the WT mice between 3 and 5 wpi correspond to the increase in IFN-γ and decline in IL-4 levels (compare Fig. 1, 2, and 4). However, considerable Arg1 expression (Fig. 2) and many Ym1/2-producing cells (Fig. 4) are still observed in the lungs at 5 wpi, while IL-13 is robustly expressed in the infected lungs (Fig. 1). Similarly, the absence of IL-4 and high levels of IFN-γ do not completely inhibit the modest/transient increase of the Ym1/2-expressing cells in IL-$4^{-/-}$ lungs, which could be attributed to the induction of IL-13 (Fig. 1). This is consistent with previous reports about the role of IL-13 (30, 31, 39).

Our final novel finding that furthers understanding of the interplay of IFN-γ and IL-4 with Mac biology comes from our *in vitro* experiment with BMM (Fig. 8). As expected, the Mac treated with IL-4 and IFN-γ induced Arg1 and iNOS proteins, respectively. Interestingly, Mac coincubated with both IFN-γ and IL-4 strongly induced both of these proteins within the same cells. Thus, unlike polarized T cells, which express either Th1 or Th2 cytokines, Mac can induce both types of activation genes simultaneously. The resultant intermediate Mac activation pattern is likely to be important not only in the pathogenesis of ABPM but also in many chronic and/or latent infections, in which a low-level pathogen survives long term "under control" of the host. Future studies are needed to evaluate the fungicidal properties of such mixed Mac, but our *in vivo* data (steady-state CFU level) suggest that these Mac may have some limited fungicidal/fungistatic properties.

Although our studies covered extensively the balance between Th1 and Th2 cytokines, studies clarifying the role of Th17 are needed to better understand cytokine interplay in chronic fungal infection. We anticipate that these studies will further our understanding of protective and nonprotective effects of cytokines in models of cryptococcal infection.

In summary, our study demonstrates that dynamic Th polarizing cytokine interplay supports chronic infection, chronic inflammation, and pathology in ABPM. Our studies also demonstrate that regulation of the Mac activation phenotype in chronic infection is controlled predominantly by IFN-γ and IL-4 balance and that the interplay between these factors, apart from aaMac and caMac, can result in formation of an intermediate activation phenotype. Since the Mac are the most distal effector cell that either eliminates *C. neoformans* or serves as an intracellular reservoir of the microbe in the infected lungs, this information may be important for future therapies aiming to "correct" the Mac activation/polarization phenotype.

ACKNOWLEDGMENTS

This work was supported by NHLBI R01-HL65912 and R01-HL63670 (G.B.H.) and VA Merit Review grants (M.A.O. and G.B.T.).

We thank Jeremy Dayrit for her assistance with proofreading of the manuscript.

REFERENCES

1. **Alspaugh, J. A., and D. L. Granger.** 1991. Inhibition of Cryptococcus neoformans replication by nitrogen oxides supports the role of these molecules as effectors of macrophage-mediated cytostasis. Infect. Immun. **59:**2291–2296.
2. **Arora, S., et al.** 2005. Role of IFN-gamma in regulating T2 immunity and the development of alternatively activated macrophages during allergic bronchopulmonary mycosis. J. Immunol. **174:**6346–6356.
3. **Beamer, G. L., et al.** 2008. Interleukin-10 promotes Mycobacterium tuberculosis disease progression in CBA/J mice. J. Immunol. **181:**5545–5550.
4. **Bhan, U., et al.** 2008. Toll-like receptor 9 regulates the lung macrophage phenotype and host immunity in murine pneumonia caused by Legionella pneumophila. Infect. Immun. **76:**2895–2904.
5. **Brys, L., et al.** 2005. Reactive oxygen species and 12/15-lipoxygenase contribute to the antiproliferative capacity of alternatively activated myeloid cells elicited during helminth infection. J. Immunol. **174:**6095–6104.
6. **Chen, G. H., et al.** 2008. Inheritance of immune polarization patterns is linked to resistance versus susceptibility to Cryptococcus neoformans in a mouse model. Infect. Immun. **76:**2379–2391.
7. **Chen, G. H., et al.** 2007. Role of granulocyte macrophage colony-stimulating factor in host defense against pulmonary Cryptococcus neoformans infection during murine allergic bronchopulmonary mycosis. Am. J. Pathol. **170:**1028–1040.
8. **Diaz, Y. R., R. Rojas, L. Valderrama, and N. G. Saravia.** 2010. T-bet, GATA-3, and Foxp3 expression and Th1/Th2 cytokine production in the clinical outcome of human infection with Leishmania (Viannia) species. J. Infect. Dis. **202:**406–415.
9. **Edwards, L., et al.** 2005. Stimulation via Toll-like receptor 9 reduces Cryptococcus neoformans-induced pulmonary inflammation in an IL-12-dependent manner. Eur. J. Immunol. **35:**273–281.
10. **El Kasmi, K. C., et al.** 2008. Toll-like receptor-induced arginase 1 in macrophages thwarts effective immunity against intracellular pathogens. Nat. Immunol. **9:**1399–1406.
11. **Fink, L., et al.** 1998. Real-time quantitative RT-PCR after laser-assisted cell picking. Nat. Med. **4:**1329–1333.
12. **Goldman, D., Y. Cho, M. Zhao, A. Casadevall, and S. C. Lee.** 1996. Expression of inducible nitric oxide synthase in rat pulmonary Cryptococcus neoformans granulomas. Am. J. Pathol. **148:**1275–1282.
13. **Goldman, D. L., S. C. Lee, A. J. Mednick, L. Montella, and A. Casadevall.** 2000. Persistent Cryptococcus neoformans pulmonary infection in the rat is associated with intracellular parasitism, decreased inducible nitric oxide synthase expression, and altered antibody responsiveness to cryptococcal polysaccharide. Infect. Immun. **68:**832–838.
14. **Granger, D. L., J. B. Hibbs, Jr., J. R. Perfect, and D. T. Durack.** 1990. Metabolic fate of L-arginine in relation to microbiostatic capability of murine macrophages. J. Clin. Invest. **85:**264–273.
15. **Granger, D. L., J. B. Hibbs, Jr., J. R. Perfect, and D. T. Durack.** 1988. Specific amino acid (L-arginine) requirement for the microbiostatic activity of murine macrophages. J. Clin. Invest. **81:**1129–1136.
16. **Hardison, S. E., et al.** 2010. Pulmonary infection with an interferon-gamma-producing Cryptococcus neoformans strain results in classical macrophage activation and protection. Am. J. Pathol. **176:**774–785.
17. **Hartl, D., K. F. Buckland, and C. M. Hogaboam.** 2006. Chemokines in allergic aspergillosis—from animal models to human lung diseases. Inflamm. Allergy Drug Targets **5:**219–228.
18. **Hernandez, Y., et al.** 2005. Distinct roles for IL-4 and IL-10 in regulating T2 immunity during allergic bronchopulmonary mycosis. J. Immunol. **174:**1027–1036.
19. **Herring, A. C., et al.** 2005. Transient neutralization of tumor necrosis factor alpha can produce a chronic fungal infection in an immunocompetent host: potential role of immature dendritic cells. Infect. Immun. **73:**39–49.
20. **Huffnagle, G. B., M. B. Boyd, N. E. Street, and M. F. Lipscomb.** 1998. IL-5 is required for eosinophil recruitment, crystal deposition, and mononuclear cell recruitment during a pulmonary Cryptococcus neoformans infection in genetically susceptible mice (C57BL/6). J. Immunol. **160:**2393–2400.
21. **Huffnagle, G. B., et al.** 1997. Macrophage inflammatory protein-1alpha (MIP-1alpha) is required for the efferent phase of pulmonary cell-mediated immunity to a Cryptococcus neoformans infection. J. Immunol. **159:**318–327.
22. **Huffnagle, G. B., et al.** 1996. Afferent phase production of TNF-alpha is required for the development of protective T cell immunity to Cryptococcus neoformans. J. Immunol. **157:**4529–4536.
23. **Jakubzick, C., et al.** 2004. Role of CCR4 ligands, CCL17 and CCL22, during Schistosoma mansoni egg-induced pulmonary granuloma formation in mice. Am. J. Pathol. **165:**1211–1221.
24. **Katakura, T., M. Miyazaki, M. Kobayashi, D. N. Herndon, and F. Suzuki.** 2004. CCL17 and IL-10 as effectors that enable alternatively activated macrophages to inhibit the generation of classically activated macrophages. J. Immunol. **172:**1407–1413.
25. **Loke, P., et al.** 2002. IL-4 dependent alternatively-activated macrophages have a distinctive in vivo gene expression phenotype. BMC Immunol. **3:**7.
26. **Manicone, A. M., K. M. Burkhart, B. Lu, and J. G. Clark.** 2008. CXCR3 ligands contribute to Th1-induced inflammation but not to homing of Th1 cells into the lung. Exp. Lung Res. **34:**391–407.
27. **Mantovani, A., et al.** 2004. The chemokine system in diverse forms of macrophage activation and polarization. Trends Immunol. **25:**677–686.
28. **Milam, J. E., et al.** 2007. Modulation of the pulmonary type 2 T-cell response to Cryptococcus neoformans by intratracheal delivery of a tumor necrosis factor alpha-expressing adenoviral vector. Infect. Immun. **75:**4951–4958.
29. **Motta, A. C., et al.** 2010. The recurrence of leprosy reactional episodes could

be associated with oral chronic infections and expression of serum IL-1, TNF-alpha, IL-6, IFN-gamma and IL-10. Braz. Dent. J. **21:**158–164.
30. **Muller, U., et al.** 2008. A gene-dosage effect for interleukin-4 receptor alpha-chain expression has an impact on Th2-mediated allergic inflammation during bronchopulmonary mycosis. J. Infect. Dis. **198:**1714–1721.
31. **Muller, U., et al.** 2007. IL-13 induces disease-promoting type 2 cytokines, alternatively activated macrophages and allergic inflammation during pulmonary infection of mice with Cryptococcus neoformans. J. Immunol. **179:** 5367–5377.
32. **Nair, M. G., D. W. Cochrane, and J. E. Allen.** 2003. Macrophages in chronic type 2 inflammation have a novel phenotype characterized by the abundant expression of Ym1 and Fizz1 that can be partly replicated in vitro. Immunol. Lett. **85:**173–180.
33. **Nishioka, Y., et al.** 2007. CXCL9 and 11 in patients with pulmonary sarcoidosis: a role of alveolar macrophages. Clin. Exp. Immunol. **149:**317–326.
34. **Olszewski, M. A., et al.** 2000. The role of macrophage inflammatory protein-1alpha/CCL3 in regulation of T cell-mediated immunity to *Cryptococcus neoformans* infection. J. Immunol. **165:**6429–6436.
35. **Osterholzer, J. J., et al.** 2009. Cryptococcal urease promotes the accumulation of immature dendritic cells and a non-protective T2 immune response within the lung. Am. J. Pathol. **174:**932–943.
36. **Raes, G., et al.** 2002. Differential expression of FIZZ1 and Ym1 in alternatively versus classically activated macrophages. J. Leukoc. Biol. **71:**597–602.
37. **Raes, G., et al.** 2005. Arginase-1 and Ym1 are markers for murine, but not human, alternatively activated myeloid cells. J. Immunol. **174:**6561; author reply, 6561-6562.
38. **Rosas, L. E., et al.** 2005. CXCR3$^{-/-}$ mice mount an efficient Th1 response but fail to control Leishmania major infection. Eur. J. Immunol. **35:**515–523.
39. **Stenzel, W., et al.** 2009. IL-4/IL-13-dependent alternative activation of macrophages but not microglial cells is associated with uncontrolled cerebral cryptococcosis. Am. J. Pathol. **174:**486–496.
40. **Ward, J. M., et al.** 2001. Hyalinosis and Ym1/Ym2 gene expression in the stomach and respiratory tract of 129S4/SvJae and wild-type and CYP1A2-null B6, 129 mice. Am. J. Pathol. **158:**323–332.
41. **Zhang, Y., et al.** 2010. TLR9 signaling is required for generation of the adaptive immune protection in Cryptococcus neoformans-infected lungs. Am. J. Pathol. **177:**754–765.
42. **Zhang, Y., et al.** 2009. Robust Th1 and Th17 immunity supports pulmonary clearance but cannot prevent systemic dissemination of highly virulent Cryptococcus neoformans H99. Am. J. Pathol. **175:**2489–2500.
43. **Zhao, J., H. Zhu, C. H. Wong, K. Y. Leung, and W. S. Wong.** 2005. Increased lungkine and chitinase levels in allergic airway inflammation: a proteomics approach. Proteomics **5:**2799–2807.

Editor: G. S. Deepe, Jr.